1 **Dopamine Induced Multiple Bonding in Hyaluronic Acid Network to**

2 **Construct Particle-free Conductive Hydrogel for Reliable Electro-**

3 **biosensing**

4 Ming-Ze Zeng [a, 1], Dan Wei [a, 1], Jie Ding [a], Yuan Tian [a], Xiao-Yang Wu [a], Zhi-Hong

5 Chen [a], Cheng-Heng Wu [a, b], Jing Sun [a], Hua-Bing Yin [c], Hong-Song Fan [a, *]

6 *[a] National Engineering Research Center for Biomaterials, College of Biomedical*

7 *Engineering, Sichuan University, Chengdu 610064, Sichuan, China*

8 *[b] Institute of Regulatory Science for Medical Devices, Sichuan University, Chengdu*

9 *610065, Sichuan, China*

10 *[c] James Watt School of Engineering, University of Glasgow, G12 8LT, U.K.*

11

12 [1] These two authors contributed equally to this work.

13

14 *** Corresponding author**

15

16 *E-mail addresses: hsfan@scu.edu.cn (H.-S. Fan)*

17

18 **Abstract**: Conductive hydrogel (CH) as flexible electrophysiology interface has

19 become the new trend of bioelectronics, but still challenging in synergizing the

20 biocompatibility, mechanics and comprehensive electrical performance. Hyaluronic

21 acid (HA), featured with abundant active sites for personalized-modification and well-

22 known biocompatibility, is one of the alterative candidates. The obstacle lies in the

23 unstable conductivity from the ionic conduction, and the electronic conduction by

24 embedding conductive nanoparticles (NPs) is likely to result in inhomogeneous CH

25 with poor stretchability and discontinuous conductive network. Herein, inspired by

catechol chemistry, dopamine (DA)-modified HA was homogeneously composited with DA-modified poly(3,4-ethylenedioxythiophene):poly(styrenesulfonate) (PEDOT:PSS, named PP), to produce particle-free conductive hydrogel (HA-DA-PP). The DA-introduced multiple bondings in HA network and PP molecules brought aqueous conductive PP into HA hydrogel to form a homogeneous crosslinking network, imparted the flexible stretchability. By accurately regulation, HA-DA-PP achieved high stretchability with large tensile deformation (over 470%) in the category of natural polymer-based hydrogels. Moreover, the interaction between DA and PP (conformational transition and charge transfer) could effectively enhance the hydrogel's conductivity. Consequently, HA-DA-PP hydrogel showed high sensibility to human movement, epidermal and *in vivo* electrophysiological signals monitoring. Overall, DA-mediated multiple bonding is a powerful strategy for constructing CH with high performance for bioelectronics.

1. Introduction

Flexible electronics get increasing attraction in personalized motion, health monitoring, rehabilitation monitoring, medical diagnosis, disease therapy and human-machine interface (Jia et al., 2021; Lin et al., 2022). Therein, interface materials as an indispensable part and the cornerstone of these devices, are of great significance (Li, Ma, & Huang, 2021). As an updating strategy of traditional metal interface with mismatched tissue mechanics and possible biotoxicity, soft interfaces featured with flexible stretchability, tissue-interface compliance and tight adhesion, as well as super electric properties (high conductivity and low impendence) are highly expected to realize precise and rapid electro-biosensing (Tang et al., 2022; Yang et al., 2019). Particularly, conductive hydrogels (CHs) are remarkable candidates for their desirable

54 mechanical flexibility and tunable conductivity (Sun, Agate, Salem, Lucia, & Pal, 2020;

55 Yazdi et al., 2021). Ionic conduction and electronic conduction are two main

56 representative strategies for designing CHs (Chen, Z. et al.). For ionic conduction-based

57 CHs, ions are easy to leak out under physiological environment, leading to unstable

58 conductivity (Yang et al., 2019). For electronic conduction-based CHs, the strategy of

59 embedding conductive nanoparticles (NPs) such as Mxene, Polypyrrole and Polyaniline

60 *etc.* within hydrogel is popular, and the possible inhomogeneous dispersion of NPs

61 might result in subsequent unavoidable stress concentration around NPs, leading to

62 interfacial mechanical mismatch, poor stretchability and unstable durability in practical

63 application (Park et al., 2019). Therefore, designing a particle-free homogeneous CH

64 has become an urgent front-burner problem to get satisfactory physical-chemical

65 performance (Song et al., 2021). Considering the possible applications for both

66 epidermal and *in vivo* monitoring with direct tissue surface contacting even long-term

67 implantation, such as neural probe for nerve activity stimuli/recording and brain-

68 machine interface signal recording, hydrogels based on synthetic polymers are hardly

69 to meet above mentioned requirements due to the inferior biocompatibility, bioactivity

70 and biodegradability (Hassan et al., 2022). Comparatively, biological derived polymers

71 such as hyaluronic acid (HA), alginate and gelatin are superior because of their native

72 biocompatibility and bioactivity (Shi et al., 2016).

73

74 HA, which is particularly abundant in natural extracellular matrix (ECM), has

75 remarkable biocompatibility, biodegradability, gelation property and customized

76 functional modification ability (Abatangelo, Vindigni, Avruscio, Pandis, & Brun, 2020).

77 In addition, HA is quite readily available and massive producible, which makes it

78 widely used in biomedical devices, including implantable scaffold and biomimetic

79 matrix for tissue regeneration (Chen, S.et al., 2021). Compared with other common

80 natural polymers such as collagen and alginate, HA contains many free active sites

81 (acetamide, carboxyl, hydroxyl and terminus aldehyde), feasible for various functional

82 modifications (Highley, Prestwich, & Burdick, 2016). The common strategy of

83 introducing chemical crosslinking bonding overcomes the HA hydrogels' weakness in

84 mechanical property and rapid degradation, whereas the conventional covalent-bonding

85 with high bond energy might suppress the mobility of HA molecular chains, leading to

86 poor stretchability. Introducing multiple bonding mode especially reversible dynamic

87 bonds as sacrificial bonds to dissipate stress is promising for improving the

88 aforementioned problems, particularly the stretchability of HA-based hydrogels (Lai,

89 2014).

90

91 There have been some attempts of using HA-based CHs in flexible bioelectronics,

92 however, most of them are dependent on the incorporation of conductive NPs, facing

93 the problem mentioned above (Liang et al., 2019; Xu et al., 2021). To get particle-free

94 HA-based CHs, introducing conductive polymers (CPs) such as polyaniline (PANI) and

95 polythiophene (PTh) seems alternative but that is still impended by the inherent

96 insolubility in water (Namsheer & Rout, 2021). Poly(3,4-ethylene dioxythiophene)

97 (PEDOT), the most popular PTh-based material, stands out among all CPs due to its

98 relatively high electrical conductivity and biocompatibility (Jeong et al., 2021).

99 Especially, poly(3,4-ethylenedioxythiophene):poly(styrenesulfonate) (PEDOT:PSS,

100 named PP) which formed by doping with hydrophilic polystyrene sulphonate (PSS),

101 successfully improved the hydrophobic of PEDOT to yield out a stable aqueous

102 dispersion (Rudd & Drew, 2022). Basing on that, a particle-free homogeneous

103 polyvinyl alcohol (PVA)-based CH has been reported (Liu et al., 2021). However, this

104 PVA-based hydrogel shows limited improvement in stretchability due to that the high

105 crystallinity of PVA leads to weak mobility of PVA chains, displaying the only

106 elongation at break of about 180.9%. In addition, the poor biocompatibility of PVA

107 hinders its further application for *in vivo* application. Hence, developing a multiple

108 bonding mode with considerable dynamic crosslinking between aqueous CPs and

109 biocompatible hydrogel matrix is highly expected.

110

The widely applied catechol chemistry inspires this possibility. With abundant phenolic hydroxyl groups, catechol derivatives can participate in noncovalent interactions, including hydrogen bonding, π-π stacking and cation-π interactions, and also undergo covalent crosslinking under oxidative conditions (Liu et al., 2014). Remarkable stretchability was reported by integrating dopamine (DA) into PVA hydrogel , which is attributed to the DA mediated multiple dynamic bonds acting as sacrificial bonds to dissipate energy (Liu et al., 2018). Moreover, literatures have reported that when DA interacts with PEDOT, the low ionization energy of PEDOT can cause the charge transfer from PEDOT to catechol/quinone groups. This charge transfer forms well-connected electric path that can enhance the conductivity of hydrogel (Gan et al., 2020). Besides, the ion replacement reaction triggered by DA doping improves the regular aggregation of PEDOT backbone, which also can enhance the conductivity (Zeng et al., 2020).

124

Hence, in this study, a novel DA-functionalized multiple bonding particle-free CH with improved stretchability, tissue-interface adhesion, self-healing ability and biocompatibility was proposed (**Scheme 1**). HA and PP were both modified by DA firstly for outputting binding sites. After that, water-soluble PP was introduced into HA to form a particle-free CH hydrogel (abbreviated as HA-DA-PP) under the oxidative coupling of catechol groups catalyzed by horseradish peroxidase (HRP) / hydrogen peroxide (H_2O_2) system. DA incorporation confers the hydrogel sufficient energy dissipation through various non-covalent interactions. PP provides conductivity for hydrogel, and the charge transfer between PEDOT and catechol/quinone groups enhances the efficiency. The proposed particle-free HA-DA-PP CH demonstrates great potential in bioelectronic applications.

136
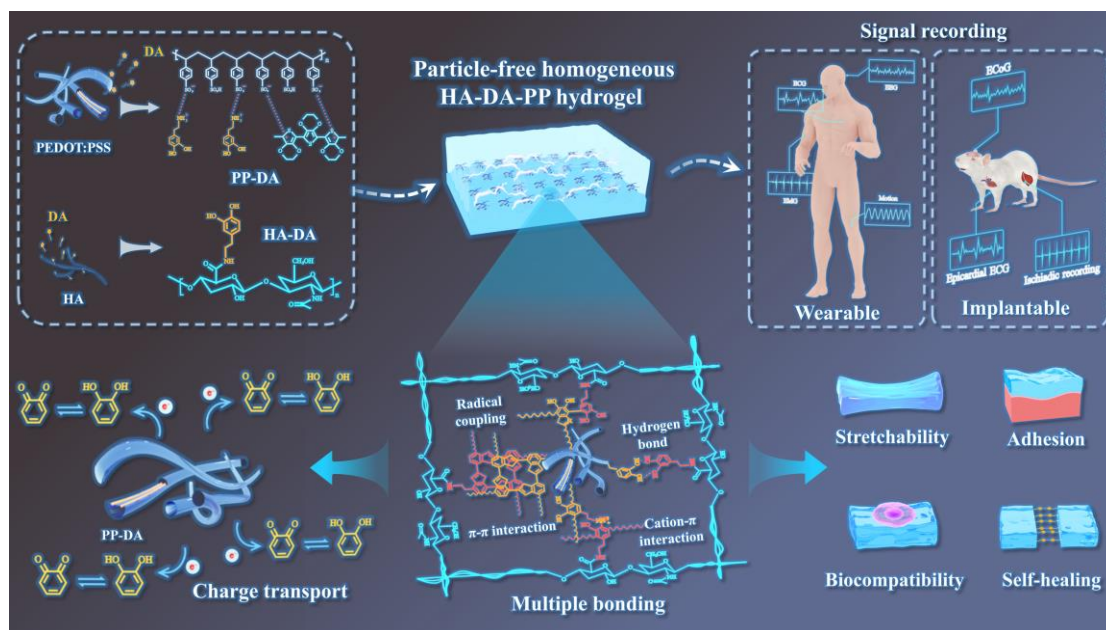
Scheme 1. The strategy of designing particle-free highly conductive HA-DA-PP hydrogel with

multiple bonding, which possesses favorable stretchability, biocompatibility, adhesion and self-

healing performance, for epidermal and *in vivo* physiological signals monitoring.

2. Materials and methods

2.1. Materials

PP was obtained from Clevios (PH1000, Germany). The 1-(3-dimethylaminopropyl)-

3-ethylcarbodiimide hydrochlorid (EDC), N-hydroxysuccinimide (NHS) and dopamine

hydrochloride (DA·HCl) were purchased from Aladdin Co. Ltd. (Shanghai, China). HA

(Mw = 700k~800k Da) was obtained from Bloomage Biotech. Co. Ltd. (Jinan, China).

Fluorescein diacetate (FDA) and propidium iodide (PI) was purchased from Sigma-

Aldrich (USA). HRP (activity: 248 unit/mg) was purchased from TCI (Japan). Unless

otherwise specified, all other chemicals were acquired from Chengdu Kelong Chem.

Co..

2.2. Preparation of PP-DA

PP-DA was synthesized via the ion exchange reaction between PSS and DA·HCl (Zeng

et al., 2020). 20 mg DA·HCl was added to PP aqueous solution (20 mL, 10 mg/mL)

6

155   directly. After half an hour stirring under room temperature (RT), the rough product was

156   obtained and further dialyzed with a dialysis membrane (1000 Da, MYM Biological

157   Technology Co. Ltd., China) for removing extra inorganic salt. The pure product PP-

158   DA (10 mg/mL) was obtained and preserved at 4°C for later use.

159

160   *2.3. Synthesis of HA-DA*

161   HA-DA was synthesized via the carbodiimide coupling chemistry (Liang et al., 2019).

162   Briefly, 1 g HA was dissolved in 100 mL of deionized water (DIW). After adjusting the

163   pH to 5 with 0.1M HCl, 440 mg EDC and 288 mg NHS were added for activating the

164   carboxy groups, then, 0.47 g DA·HCl in 5 mL DIW was added, stirred overnight at RT

165   under nitrogen protection. Subsequently, the reaction solution was dialyzed against

166   DIW with a dialysis membrane (10,000 Da) for 3 days and lyophilized to obtain pure

167   product HA-DA, then analyzed by ^{1}H NMR spectrum (600 MHz, Bruker, USA).

168

169   *2.4. Preparation of HA-DA-PP hydrogel*

170   To form a series of HA-DA-PP hydrogels, HA-DA solution (2.5 wt%) and PP-DA

171   solution with various concentration (0, 0.2, 0.5 and 1 mg/mL, respectively) were mixed,

172   followed by adding 12.5 μL of H_2O_2 (0.5 mol/L) and 30 μL of HRP solutions (1mg/mL).

173   The final obtained hydrogels were noted as HA-DA (without PP-DA), HA-DA-PP0.2,

174   HA-DA-PP0.5 and HA-DA-PP1, respectively. As control, HA-DA@PP0.5 was

175   prepared by adding 0.5 mg/mL PP (without DA modification) into 2.50 wt% HA-DA

176   solution.

177

178   *2.5. Characterization of interaction between DA and PP in PP-DA*

179   The content of PEDOT and PSS domain in PP and PP-DA was analyzed using X-ray

180   photoelectron spectroscopy (XPS) (AXIS SUPRA, Kratos, UK). The chemical

181   structure of PP and PP-DA was analyzed with Raman spectroscopy (inVia Raman

182   microscope, Renishaw, UK). The Atomic Force Microscope (AFM) (Dimension Icon,

183   Bruker, Germany) was used to characterize the morphology. The radical character of

184   PP-DA and PP was detected using the electron spin resonance (ESR) test (JES X310,

185   JOLE, Japan). The cyclic voltammetry (CV) curve and conductivity of PP and PP-DA

186   were tested using the CHI 660E electrochemical workstation (ChenHua, China).

187

188   *2.6. Physical-chemical characterization of hydrogels*

189   *2.6.1. Hydrogel homogeneity:* Tunneling-AFM (TUNA) with a contact mode on

190   Dimension Icon (Bruker, Germany) was used to characterize the morphology and

191   distribution of PP-DA in composite hydrogels. As control, HA-DA@P0.5 was prepared

192   by adding 0.5 mg/mL PEDOT NPs (without PSS) into 2.50 wt% HA-DA solution.

193

194   *2.6.2. Gelation kinetics:* The rheological behavior was measured via dynamic

195   oscillatory shear rheometry (TA Instruments, USA) under a strain of 1% and 1 Hz. Five

196   parallel samples per group were tested.

197

198   *2.6.3. Swelling test:* Hydrogels (diameter = 5 mm; height = 2 mm) were lyophilized and

199   soaked in phosphate-buffered saline (PBS, pH 7.4) at 37 °C. At predetermined time

200   intervals, the swollen hydrogels were weighted after removing excess water with filter

201   paper. The swelling ratio (SR) was calculated using the following equation 1 (Eq 1):

202      $$SR = \frac{W_t - W_0}{W_0} \times 100\% \qquad\qquad\qquad (1)$$

203   Where W_0 and W_t represent the original dry-weight and the changed weight of the

204   hydrogel at time t, respectively.

205   Five parallel samples per group were tested.

206

207   *2.6.4. Degradation test:* Hydrogels were soaked in the medium at 37 °C and changed

208   every day. At the predetermined time, the hydrogels were taken out and weighted. The

209   mass remaining (MR) was calculated using the following equation 2 (Eq 2):

210 $$MR = \frac{W_t}{W_0} \times 100\% \qquad\qquad\qquad (2)$$

211 Where W_0 and W_t represent the original wet-weight and the changed weight of the

212 hydrogel at time t, respectively.

213 Five parallel samples per group were tested.

214

215 *2.6.5. Morphology characterization:* All hydrogels (diameter = 5 mm, height = 2 mm)

216 were lyophilized and exposed the cross section. Scanning electron microscopy (SEM,

217 S-4800, Hitachi, Japan) was adopted to investigate the interior morphology of the

218 hydrogels at an acceleration voltage of 3.0 kV. ImageJ software (NIH, USA) was used

219 to evaluate the pore size of hydrogels. Five parallel samples for each group were used.

220

221 *2.6.6. Mechanical characterization:* The compressive stress-strain curve of the

222 hydrogel samples (diameter = 5 mm, height = 2 mm) was obtained at a strain rate of 1

223 mm/min with a dynamic mechanical analyzer (DMA, TA Q-800, USA) under RT. The

224 compressive modulus was defined as the slope of the linear region from 0 to 10% strain.

225 For tensile strength test, the hydrogels were formed in a cube mold (5 mm × 20 mm ×

226 2 mm), then tested with DMA at an extension speed of 20 mm/min. Five parallel

227 samples per group were assessed and the resulting values were averaged.

228

229 *2.6.7. Measurement of adhesion strength:* The adhesive strength of HA-DA-PP

230 hydrogels was determined by lap-shear test using DMA. Prior to test, fresh porcine skin

231 was prepared by removing adipose tissue layer and cut into rectangular shape (length =

232 3 cm, width = 1 cm). Then, 100 μL of precursor solution was applied to the inner surface

233 of two pieces of porcine skins to cover 1 cm × 1 cm overlapping region. After gelation,

234 adhesive-applied skin samples were measured with DMA at a loading speed of 5

235 mm/min. All measurements were repeated five times.

236

237　*2.6.8. Self-healing performance:* HA-DA-PP hydrogel was cut into halves and put

238　together without external treatments. Then we pulled the separated parts with tweezers.

239　Further, the self-healing performance was also assessed by the alternating step strain

240　scanning mode (50% and 2500% oscillation strain) during five cycles using DMA at

241　37 °C with 1 Hz frequency.

242

243　*2.7. Biocompatibility evaluation*

244　To investigate the biocompatibility, 3T3 cells were firstly inoculated to a 48-well plate

245　at a density of 5000 cells per well. After cells completely adhering, HA-DA-PP

246　hydrogels were placed in culture plate. Live/Dead staining and MTT were carried out

247　to evaluate cell viability and proliferation according to the protocol. FDA imaging was

248　observed by confocal laser scanning microscope (CLSM, Leica-TCSSP5, Germany) .

249　For *in vivo* biocompatibility, HA-DA and HA-DA-PP hydrogel (diameter of 5mm and

250　height of 2 mm) were implanted in the dorsal subcutaneous area of SD rat (female), and

251　silver wire (diameter of 0.3 mm and length of 5 mm) were implanted as control. The

252　subcutaneous area of the implant site of three groups was excised after 14 days of

253　implantation and fixed in 10 % formalin for 24 h, then followed by hematoxylin-eosin

254　(HE) staining. The experimental protocols were performed in accordance with the

255　ARRIVE guidelines, and all animal experiments were strictly performed with the

256　National Research Council's Guide for the Care and Use of Laboratory Animals and

257　approved by the Sichuan Provincial Committee for Experimental Animal Management

258　(approval number: SYXK (Sichuan): 138 2019-189).

259

260　*2.8. Electrochemical properties measurement*

261　Electrochemical impedance spectroscopy (EIS), CV and Nyquist curve of the hydrogels

262　were carried out using an electrochemical workstation (Reference 600, Gamry

263　Instruments, USA) equipped with the linear four-pin probe (ST2558B-F01, Suzhou

264　Jingge, China). The conductivity (σ) of the hydrogels was measured with a digital

265 source meter (2612B, Keithley, USA) by two-point method, then evaluated by Eq. 3.

266 $$\sigma = \frac{L}{RS} \tag{3}$$

267 Where L, R and S represent the length, electrical resistance and cross-sectional area of

268 the sample, respectively.

269

270 *2.9. Electromechanical properties measurement*

271 The electromechanical properties of hydrogels were tested via the digital source meter

272 under dynamic stretching with the uniaxial tensile tester (BioTester, Canada). Gauge

273 factor (GF) was evaluated by Eq. 4.

274 $$GF = \frac{\Delta R/R_0}{\Delta \varepsilon} \tag{4}$$

275 Where ΔR, R_0, and $\Delta \varepsilon$ were represent the changed resistance with strain, starting

276 resistance, and applied strain, respectively.

277

278 *2.10. Human motion monitoring*

279 For human motion monitoring, all related experiments had been carried out in

280 accordance with The Code of Ethics of the World Medical Association (Declaration of

281 Helsinki). The volunteer who participated in the experiment was obtained the informed

282 written consent prior to research, and all the experiments were approved by the Medical

283 Ethics Committee of Sichuan University (KS2022863). In detail, the HA-DA-PP1

284 hydrogels (also called as HDP in the text) were attached onto a volunteer's finger, wrist

285 and knee, respectively. The white bandages were used to fix the wires that connecting

286 the hydrogel and a digital source meter for transmitting electrical signals and the R-t

287 curves were recorded.

288

289 *2.11. Electrophysiological signals monitoring*

290 Epidermal electrophysiological signals, including electromyography (EMG),

291   electrocardiogram (ECG) and electroencephalogram (EEG) were detected. The EMG

292   signal was obtained with an EMG signal tester (TeleMyo2400 T, Noraxon, USA),

293   therein, the HDP hydrogel was filled into a commercial button-like electrode, and three

294   HDP-contained hydrogel electrodes were attached to the muscle peak of biceps brachii,

295   medial acromion and fossa cubit of a volunteer, respectively. To obtain the ECG signal,

296   two HDP-contained hydrogel electrodes were connected to the wireless Bluetooth

297   module (BMD101, Xinweilai, China) then adhered onto the mid left of a volunteer's

298   chest. To obtain the EEG signal, a 64-channel EEG-cap was used of which reference

299   and ground placing above volunteer's nose. HDP hydrogel and commercial Ten20$^{®}$

300   Conductive Paste (control, 10-20-4，Weaver and company, USA) were filled into the

301   two channels of the EEG-cap, respectively. The EEG signals were recorded by an EEG

302   signal detector (SynAmps RT 64-channel, Neuroscan, USA). For *in vivo*

303   electrophysiological signals monitoring, a female SD rat was used as the animal model.

304   Sciatic signal, epicardial ECG and ECoG signals were recorded by a multichannel

305   neural signal recording system (BlackRock, Cereplex Direct, USA), respectively. For

306   sciatic signal, the HDP hydrogel was wrapped on sciatic nerve and the two references

307   were attached on rat's tail and gastrocnemius, respectively. For epicardial ECG, the

308   HDP hydrogel was attached on epicardium and the reference was attached on rat's tail.

309   For ECoG signal, the HDP hydrogel was attached the primary visual cortex in the left

310   hemispheres of a rat, and the reference was attached on the dura mater. The

311   experimental protocols were performed in accordance with the ARRIVE guidelines,

312   and the animal experiments were strictly performed with the National Research

313   Council's Guide for the Care and Use of Laboratory Animals.

314

315   *2.12. Statistical analysis*

316   Unless otherwise specified, all data are expressed as mean ± standard deviation (SD).

317   One-way analysis of variance (ANOVA) was applied to perform the statistical analysis

318   among the multiple groups. Statistically significant was indicated by $*p < 0.05$, $**p <$

319   0.01, and ***p < 0.001.

320

321   **3. Results and discussion**

322   *3.1. Preparation and physical-chemical characterization of HA-DA-PP hydrogel*

323   The preparation process of particle-free conductive HA-DA-PP hydrogel is shown in

324   **Figure 1**. Firstly, DA was introduced into PP via electrostatic interaction between

325   primary amine group on DA and sulfonic acid ions on PSS to obtain PP-DA (**Figure**

326   **1A**), which can be subsequently combined into HA hydrogel network through the

327   oxidative polymerization of catechol groups. The ^{1}HNMR spectra of PP-DA and PP in

328   **Figure 1B** shows the successful introduction of DA by the characteristic peaks of

329   protons in the catechol ring and -CH$_2$- group close to the catechol ring (marked 1, 2, 3,

330   4, 5, 6) within PP-DA (Zeng et al., 2020). The absorption band at around 800 nm of

331   UV-vis absorption in **Figure S1** further confirmed the successful preparation of PP-DA

332   (Huang et al., 2017). HA-DA was synthesized by carbodiimide coupling chemistry

333   (**Figure 1C**), which was confirmed by the appearance of catechol proton peaks around

334   6.7 ppm (marked a, b, c) and proton peak of -CH$_2$- group close to the catechol ring at

335   2.76 ppm. (marked d,e) in ^{1}HNMR (**Figure 1D**) (Liang et al., 2019; Xu et al., 2021).

336   According to ^{1}HNMR, the grafting rate of HA-DA and PP-DA were calculated to be

337   21.9% and 46.4% respectively. Homogeneous HA-DA-PP hydrogel was formed via

338   generation of catechol−catechol adducts between HA-DA and PP-DA triggered by

339   H$_2$O$_2$ and HRP under neutral conditions **(Figure 1E, S2)**. Additionally, covalent

340   crosslinking between DA and amine groups, and non-covalent interactions like

341   hydrogen bonds from catechol's –OH groups, π–π electron interaction with benzenes,

342   and cation-π interaction between NH$_3^+$ and benzenes also contributed to hydrogel

343   network formation. The homogeneity of HA-DA-PP hydrogel could be demonstrated

344   by the distribution of conductive phase in HA-DA hydrogel using tunneling-AFM

345   (TUNA) conductivity map at the micro-scale level (Song et al., 2021). As **Figure 1F**

346   shown, an ultra-uniform conductivity with a wide range of conductive paths was found

347 in HA-DA-PP hydrogel, which proved the successful formation of homogeneous
348 conductive hydrogel network. Contrary to that, in the control group of HA-DA@P
349 hydrogel by adding PEDOT NPs into HA-DA hydrogel, the TUNA conductivity map
350 showed obvious PEDOT NPs aggregation, which should be attributed to the lack of
351 chemical interaction within hydrogel molecular chains **(Figure 1G)**. That is to say, the
352 DA-introducing helped the formation of homogeneous particle-free CH.

353
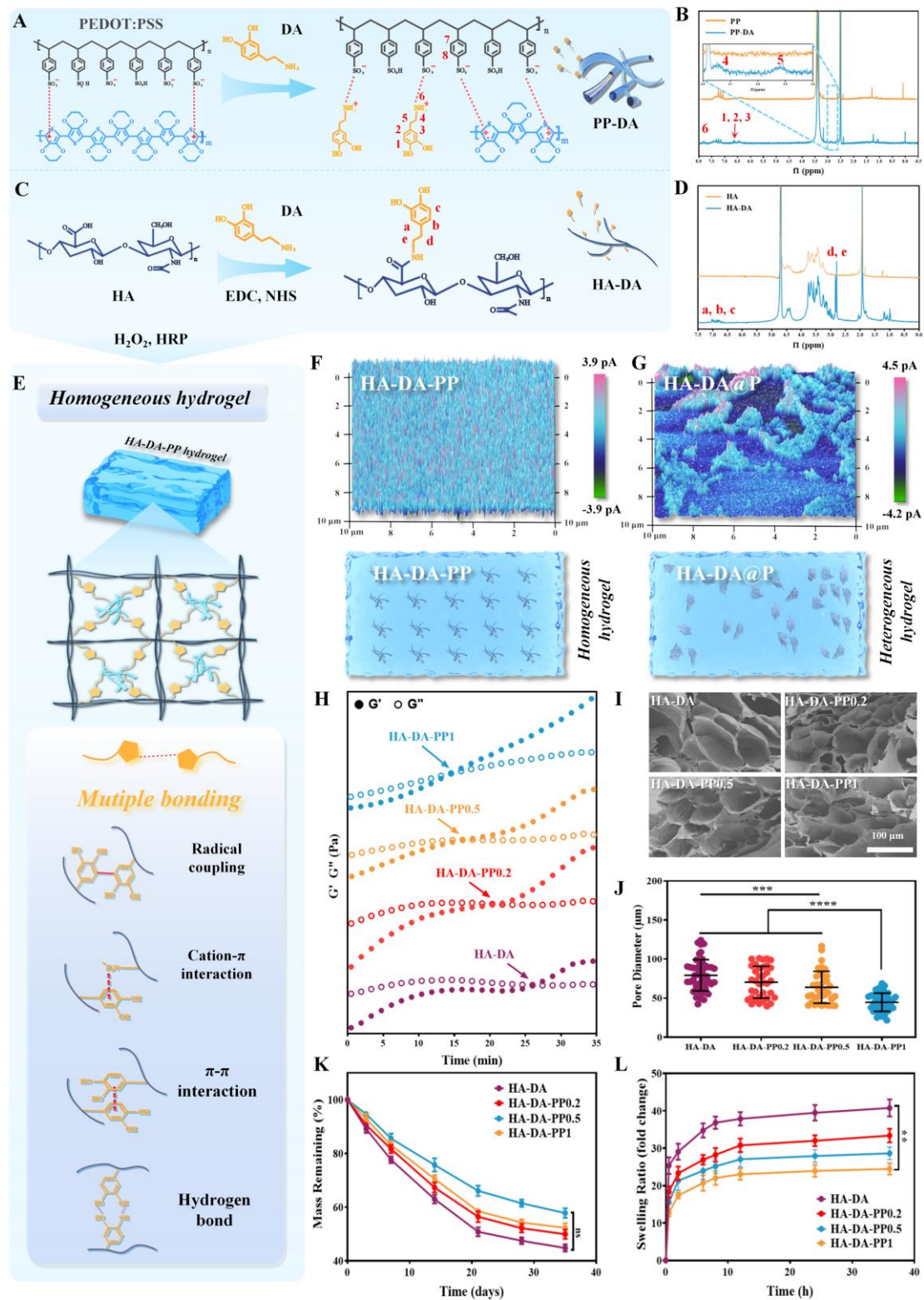
Figure 1. Preparation and characterization of HA-DA-PP hydrogels. A) Preparation of PP-DA; B)

the ^{1}HNMR spectra of PP-DA and PP; C) preparation of HA-DA; D) the ^{1}HNMR spectra of HA-

DA and HA; E) preparation of homogeneous HA-DA-PP hydrogel with multiple bonds initiated by catechol chemistry; TUNA conductivity mapping (upper) and distribution schematic (bottom) of F) HA-DA-PP and G) HA-DA@P hydrogel; Characteristics of HA-DA-PP hydrogels with various PP-DA concentration. H) Rheological behavior; I) SEM images; J) pore size distribution (n = 5); K) swelling ratio in PBS at 37 ℃; L) degradation curves in culture medium at 37 ℃.

We further investigated the influence of PP-DA concentration on HA-DA-PP hydrogels' physicochemical properties. The gelation time of HA-DA-PP hydrogels was assessed with various PP-DA concentration (0, 0.2, 0.5 and 1 mg/mL), named as HA-DA, HA-DA-PP0.2, HA-DA-PP0.5 and HA-DA-PP1, respectively. As shown in **Figure 1H**, pure HA-DA hydrogel took over 25 mins to reach the gelation point. While the introducing of PP-DA significantly shortened the gelation time, ranged from 20.6 mins of HA-DA-PP0.2 to 10.3 mins of HA-DA-PP1. Apparently, PP-DA containing catechol groups accelerated the formation of hydrogel network. Compared with HA-DA, the gelation time of HA-DA@PP0.5 (hydrogel with 0.5 mg/mL PP, without DA doping) varied little, which should be attributed to the lack of catechol groups on PP molecule (**Figure S3**). Like most polysaccharides-based hydrogels, HA-DA-PP hydrogels showed the interconnected honeycomb structure (**Figure 1I**) and the pore size decreased with PP content (**Figure 1J**). Moreover, the pore size in HA-DA-PP0.5 was smaller than that of HA-DA@PP0.5, which also confirmed that the DA modification against PP contributes to hydrogel network formation, resulting in denser interior structure (**Figure S4**). **Figure 1K** and **Figure 1L** show the swelling ratio and degradation ratio decreased with the increasing of PP-DA concentration, verifying that PP-DA content is beneficial to generate multiple bonding within hydrogel network, accompanied by the shortened gelation time and denser interior structure.

3.2. Mechanical, adhesive, self-healable and electrical properties of HA-DA-PP hydrogel

384   Appropriate mechanical properties, including elastic modulus and tensile strength,

385   adhesive property and self-healing capability are prerequisites of flexible electronics to

386   prevent them falling off tissue surface during application. DA-introduced multiple

387   bonding has a crucial effect on the mechanical property. As expected, compared to HA-

388   DA hydrogel, HA-DA-PP hydrogels showed enhanced compressive modulus, which is

389   positively related to PP-DA concentration. HA-DA-PP1 possessed the highest

390   compressive modulus of 2.51±0.17 kPa, nearly double that of HA-DA hydrogel (**Figure**

391   **2A**). Besides, HA-DA-PP1 hydrogel also showed a larger tensile deformation with a

392   higher breaking strength (over 470%), and the hydrogel adhered to the fingers could be

393   stretched to more than 3 times compared to its initial length along with the fingers'

394   separation, indicating the good flexible stretchability (**Figure 2B&C**). The improved

395   mechanical properties of HA-DA-PP hydrogels also can be attributed to the multiple

396   bonding formed in the hydrogel network. Owing to the presence of polar groups like

397   amine ($-NH_2$) and hydroxy (-OH), it was expected that the HA-DA-PP hydrogels

398   possessed excellent tissue adhesive ability (**Figure 2D**), which was confirmed by the

399   lap-shear test. As **Figure 2E** shown, the introduction of PP-DA leaded to improved

400   adhesion property, ranged from 7.51±0.79 kPa of HA-DA to 13.3±0.79 kPa of HA-

401   DA-PP1. **Figure 2F** further shows that the HA-DA-PP1 hydrogel can adhere on the

402   moist tissue surface then peel off completely without any residue, showing its *in vivo*

403   application potential. The HA-DA-PP hydrogels also showed unique self-healing

404   property due to the widely interactions including catechol−catechol adducts and

405   dynamic noncovalent interactions (**Figure 2G**). As shown in **Figure 2H**, the two-cut

406   HA-DA-PP1 hydrogel species were able to self-heal efficiently and tolerated 3 times

407   stretching after 30 minutes of contact. Rheology test evaluated the self-healing behavior

408   of HA-DA-PP1 hydrogel under 50% and 2500% strain for the cyclic testing (**Figure**

409   **2I**), which showed that the storage modulus (G′) drastically reduced and was lower than

410   loss modulus (G″), suggesting the disruption of hydrogel network. When the strain

411   switched to 50%, the G′ and G″ became higher and the G′ was higher than G″,

indicating the recovery of hydrogel network. Even after four cycles, there was no

significant variation in G′ and G″, and the self-healing hydrogel showed the similar

maximum tensile deformation as the original hydrogel (**Figure S5**), confirming the

excellent self-healing property of HA-DA-PP hydrogel. Moreover, the HA-DA-PP

hydrogels with time-dependent viscosity endowed them good viscosity (**Figure S6**),

which is helpful for *in vivo* detection.
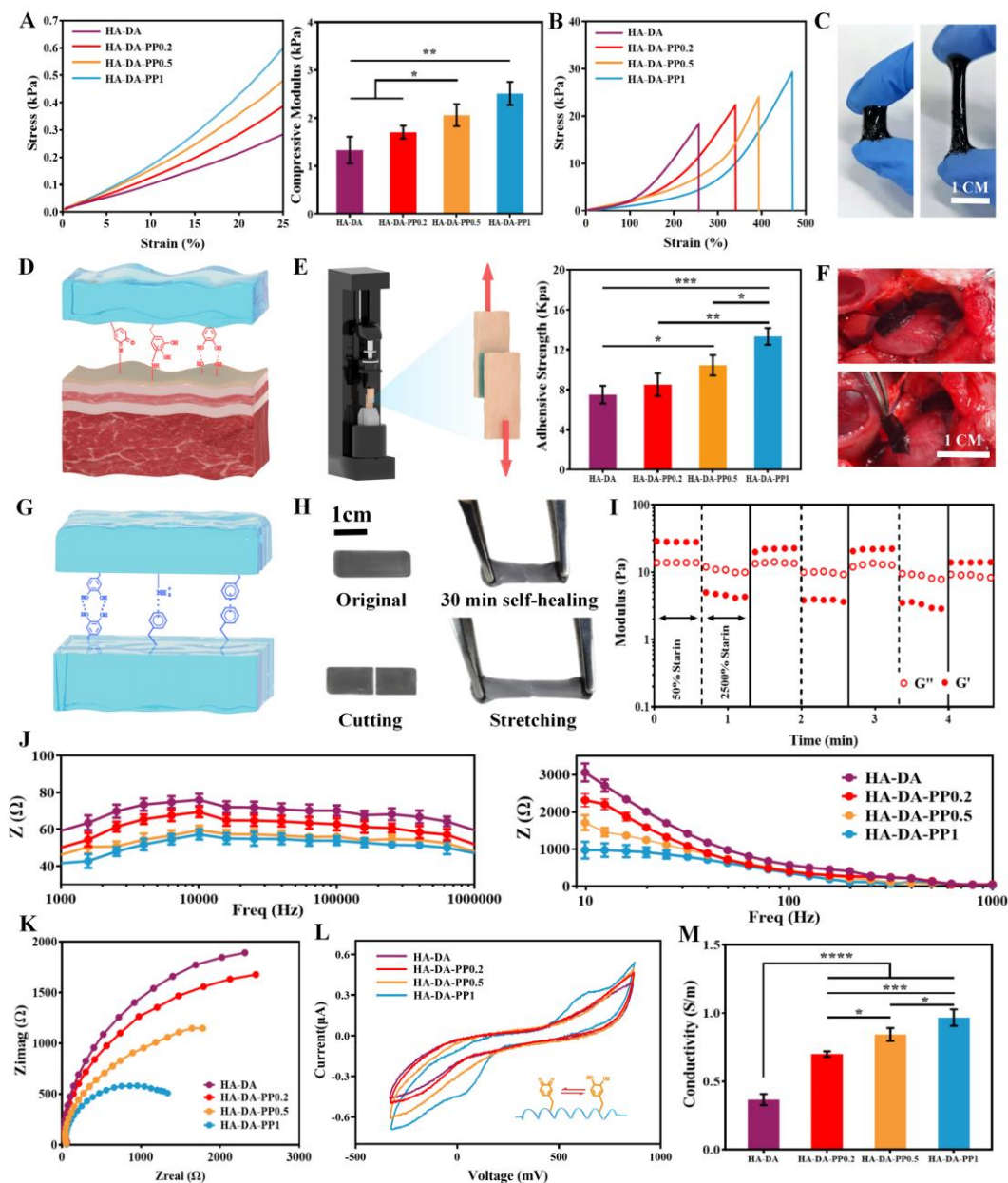
Figure 2. Mechanical properties, tissue adhesion, self-healing properties and electrochemical

properties of the hydrogels. A) The stress-strain curves (left) and compressive modulus (right) under

1

421   compression mode (n = 5); B) the stress-strain curves under tensile mode; C) uniaxial stretching of

422   HA-DA-PP1 hydrogel; D) schematic of hydrogel-tissue interface interaction; E) design of lap-shear

423   test and the adhesion strength of the hydrogels; F) image of HA-DA-PP1 hydrogel adhering to the

424   heart of a rat followed by easily peeling; G) schematic of multiple dynamic bonding participating

425   in hydrogel's self-healing; H) the macroscopic self-healing presentation of HA-DA-PP1 hydrogel;

426   I) alternate step strain sweep test (50% and 2500%) of HA-DA-PP1 hydrogel; J) electrical

427   impedance spectroscopy (EIS) of the hydrogels from 100 Hz to 10 MHz; K) Nyquist curves of four

428   hydrogels; L) CV curve of four hydrogels; M) conductivity of four hydrogels (n = 5).

429

430   Ideal electrochemical properties of CHs for reliable electrical signal recording is also

431   necessary for bioelectronics applications (Li et al., 2022). Electrical impedance

432   spectroscopy (EIS) results revealed a lower alternating current (AC) impedance of HA-

433   DA-PP hydrogels than HA-DA, ranging from 100 Hz to 10 MHz due to the introduction

434   of conductive component PP-DA, and the value was negatively correlated to PP-DA

435   concentration (**Figure 2J**). **Figure 2K** shows the Nyquist curves, in which the diameter

436   of the semicircles decreased with the increasing of PP-DA concentration, indicating the

437   decrescent impedance with higher PP-DA. The CV curves showed the enhancement of

438   oxidative and reductive peak at around 640 mV and 45mV with the increase of PP-DA

439   content, corresponding to the transition between catechols and quinones (**Figure 2L**).

440   As the electron donor and acceptor complex composed of PEDOT and DA was formed

441   in HA-DA-PP, the transition of quinones to catechols could promote the charge transfer

442   between PEDOT and catechol/quinone groups on DA (details will be discussed in the

443   next section). The charge transfer further facilitated the formation of well-connected

444   electric path in HA-DA-PP hydrogels (Zeng et al., 2020). More intuitively, the

445   conductivity of the HA-DA-PP hydrogels increased from 0.7 S/m of HA-DA-PP0.2 to

446   0.97 S/m of HA-DA-PP1, which were considerably higher than HA-DA (**Figure 2M**).

447   The improved conductivity of HA-DA-PP is attributed to the introduction of conductive

448   phase and the formed well-connected electric path via charge transfer (Gan et al., 2020).

449 The high conductivity of HA-DA-PP1 hydrogel was further proved by lighting up a

450 LED light in a 9V DC circuit (**Figure S7**). Predictably, owing to PP-DA introduction,

451 the elevated hydrogel performance (high stretchability, self-healing and adhesivity) and

452 conductivity would be beneficial for electrical signals transmission for flexible

453 bioelectronics in electro-biosensing applications.

454

455 *3.3. Interaction between DA and PP*

456 In order to investigate relationship between the enhanced electrical properties and the

457 addition of PP-DA within HA-DA-PP hydrogel, we further investigated the interaction

458 between DA and PP. Based on previous literatures, we speculated that DA was

459 introduced into PP molecule chain by the electrostatic interaction between primary

460 amine group on DA and sulfonic acid ions on PSS, which would lead to the phase

461 separation of PEDOT (conductive part) and PSS (non-conductive part). The phase

462 separation may further improve the regular aggregation of PEDOT domain and

463 benzenoid-to-quinoid conformation transition of PEDOT, which finally promoted the

464 electrical properties of PP-DA within HA-DA-PP hydrogel (Won et al., 2022) **(Figure**

465 **3A)**. In addition to this conformational transition hypothesis, we also came up with

466 another hypothesis of charge transfer between DA and PEDOT part within the entire

467 PP (Huang et al., 2017) **(Figure 3B)**.

468

469 The conformational transition was characterized by the structural changes of PP after

470 DA doping via XPS analysis. The XPS spectrograms of PP and PP-DA in **Figure 3C**

471 (gray line) can be separated into two peaks of PEDOT domains between 167 and 162

472 eV (blue line) and two peaks of PSS domains (the S(2p) peaks of sulfur atoms) between

473 172 to 164 eV (orange line), and decreased PSS area and increased PEDOT area was

474 observed from PP to PP-DA. The PEDOT/PSS area ratio of pure PP was 0.316 and that

475 of PP-DA was 0.389 (**Figure 3D**), which further demonstrated more regular

476 aggregation of conductive PEDOT-rich domains in PP-DA. In general, the formation

477   of PEDOT-rich domains is accompanied by the increase of PEDOT crystallinity and

478   benzenoid to quinoid transformation (Won et al., 2022). Subsequently, Raman

479   spectroscopy was performed to investigate the molecular state of PEDOT domain in PP

480   and PP-DA (**Figure 3E**). PEDOT exhibited typical quinoid structure (1410 cm^{-1}) and

481   benzoid structure (1436 cm^{-1}). By comparing the area of quinoid and benzoid structure,

482   the quinoid/benzoid ratio of PP-DA (2.188) was found significantly higher than that of

483   PP (1.137), indicating more quinoid structure in PP-DA (**Figure 3F**). The conductive

484   mechanism of PEDOT is related to the delocalization of the oxidation-prone π-electrons

485   on the thiophene ring (Le, Kim, & Yoon, 2017). Upon oxidation, π-electrons would

486   detach from the initial PEDOT chain, then form unstable delocalized electrons. To

487   stabilize extra energy form delocalized electrons, PEDOT would trigger conformational

488   transition from the benzenoid structures (low energy state) to the quinoid ones (high

489   energy state) to dissipate the extra energy. During this process, PEDOT would produce

490   polarons (with single electron) or bipolar polarons (with double electrons) to act as

491   charge carriers. Hence, PP-DA with more quinoid structure possessed higher electrical

492   conductivity, because more charge carriers favor the formation of well-connected

493   electric path. The varied morphology in AFM mapping of PP (amorphous cluster

494   structure) and PP-DA (extended linear structure) also reflected the different

495   benzenoid/quinoid composition within these two samples **(Figure 3G)** (Fan et al.,2019).

496   Above results verified benzenoid-to-quinoid conformation transition hypothesis caused

497   by DA doping, which further improves the conductivity of PP-DA.

498

499   The charge transfer between DA and PEDOT was verified by the ESR test. As shown

500   in **Figure 3H**, more obvious ESR signal in PP-DA compared to PP confirmed the

501   formation of DA semiquinone radical in PP-DA. Meanwhile, the delocalized electrons,

502   which exited on the molecular skeleton of PEDOT, preferred to transfer to DA

503   semiquinone radical with electron-withdrawing property (Zeng et al., 2020). The charge

504   transferring between PEDOT and DA was further directly confirmed by CV analysis in

Figure 3I, which showed none obvious oxidation peaks in PP while a pronounced oxidation peak at a potential around 1.2 V in PP-DA. By DA doping, a quasi-reversible redox process occurred in PP-DA, which confirmed the interaction of charge transfer between PEDOT and DA. Hence, due to conformational transition and charge transfer effect, PP-DA showed higher (about 4 folds) conductivity than that of pure PP (**Figure 3J**).

In summary, the interaction between DA and PP, including conformational transition and charge transfer effects, contributes the well-connected electric path formed in the hydrogel, leading to more electrons to move along the polymer chains and enhances the conductivity of HA-DA-PP hydrogels.
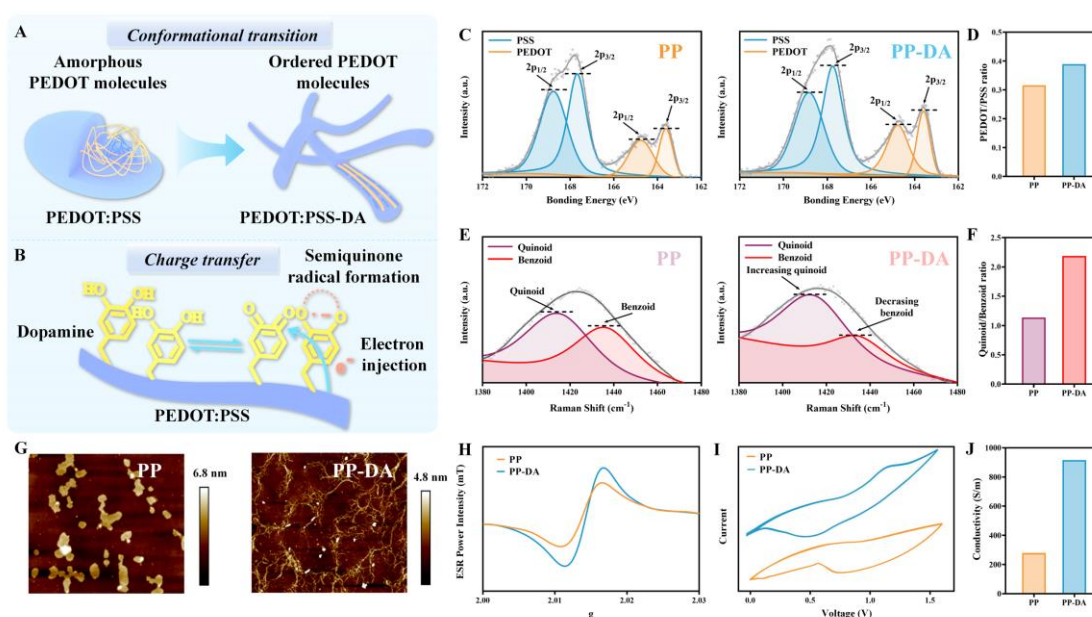
Figure 3. Interaction between DA and PP for enhanced conductivity. A) The schematic of conformational transition of PEDOT domines after DA doping; B) the schematic of charge transfer effect between PEDOT and DA; C) XPS results of PP and PP-DA; D) PEDOT/PSS ratio of PP and PP-DA; E) Raman spectroscopy results of PP and PP-DA; F) quinoid/benzoid ratio of PP and PP-DA; G) AFM image of PP and P-DA; H) ESR spectra of PP and PP-DA; I) CV curves of PP and PP-DA; J) conductivity of PP and PP-DA.

3.4. Electromechanical property and human motion monitoring

With superior conductivity and flexible stretchability, HA-DA-PP1(hereinafter referred to as HDP) hydrogel was selected for following human motion monitoring applications. **Figure 4A** shows the flow chart of electromechanical property test of the hydrogel under dynamic stretching mode. The typical trend of $\Delta R/R_0$ versus tensile strain of the HDP hydrogel in **Figure 4B** showed the markedly linear rise in relative resistance, indicating good electromechanical response. This trend could be explained by the increased tensile strain leading to decreased contact area of PP-DA, which finally reduces hydrogel conductivity as extended tunneling of electron transfer. The value of $\Delta R/R_0$ increased with incremental tensile strains **(Figure 4C)**, 1.86% of 5% tensile strain to 39.23% of 50% tensile strain, and recovered once the tensile stress was withdrawn, also indicating favourable electromechanical sensitivity of HDP. Next, $\Delta R/R_0$ under different dynamic loading frequency from 0.01 to 1Hz with a fixed 20% strain was revealed **(Figure 4D)**. Under all frequencies, the value of $\Delta R/R_0$ raised and then descended, showing the excellent strain-sensitive electrical repeatability of HDP. Moreover, this hydrogel could bear over 150 cycles under 50% strain with well-preserved $\Delta R/R_0$ amplitude (**Figure 4E**). The conductivity restoration of CH was also important for bioelectrical signals sensing and recording. **Figure 4F** shows the resistance variation of HDP during two cutting–healing cycles. The resistance became extremely high after cutting off, then dropped sharply and gradually recovered to original value within only 110 ms. Such electrically self-healable property is derived by the association of multiple dynamic bonds, leading to the seamlessly healing of the dissected hydrogel in a relatively short time (Ge et al., 2019). When the finger gently pressed the hydrogel, the resistance quickly declined within 82.5 ms (**Figure 4G**) which is relatively shorter than previously reported pressure sensors (Huang et al., 2020; Pang et al., 2018). The real-time accuracy of this designed hydrogel for electrical signals recording is beneficial to further human motion monitoring.

552   As a proof of concept, we revealed the real-time human motion monitoring using HDP.

553   **Figure 4H** shows the resistance variation of HDP on the finger with repeatedly

554   bending–relaxing for 5 times, and it can be found that the resistance was precise and

555   repeatable during the entire process. Besides, the resistance variation changed in

556   accordance with the amplitude of finger's movement (**Figure 4I**). **Figure 4J** shows that

557   making different expressions like frowning and astonishment also could trigger

558   corresponding resistance changes. Similarly, subtle and complex muscle movements

559   involved in speaking different words such as "e-skin", "hydrogel" and "sensor" could

560   be detected along with distinguishing resistance signal changes (**Figure 4K**). Notably,

561   the HDP hydrogel could be reused for electromechanical signal recording after self-

562   healing, showing a real-time responsive $\Delta R/R_0$ changing on wrist and knee after self-

563   healing (**Figure 4L&M**). These results suggested the huge potential of HDP hydrogel

564   as strain sensors for human motion monitoring.
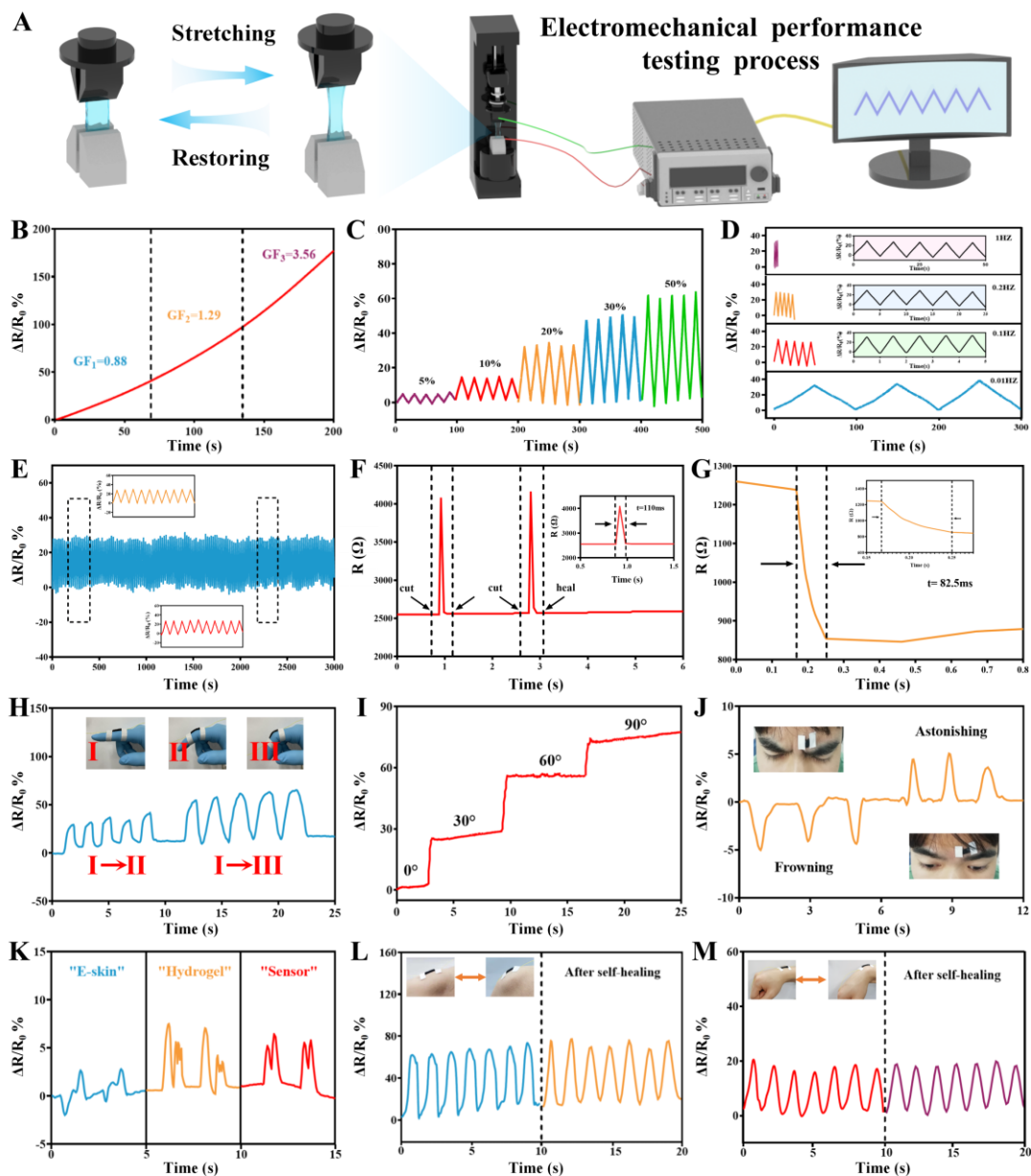
Figure 4. Electromechanical properties of HDP (HA-DA-PP1) hydrogel and human motion monitoring. A) Schematic diagram of the electromechanical performance testing process; B) $\Delta R/R_0$ curve of the HDP hydrogel under applied strain; C) $\Delta R/R_0$ curve of HDP hydrogel under five cycles from low strain to high strain; D). $\Delta R/R_0$ curve of HDP hydrogel at different frequencies and fixed 50% strain; E) $\Delta R/R_0$ curve of HDP hydrogel under 150 cycles; F) resistance change of HDP hydrogel during periodic cutting and self-healing; G) resistance change of HDP hydrogel when a finger pressing; time-dependent resistance variations during H) index finger bending-unbending in a cycle and I) maintaining the certain angle (0°, 30°, 60° and 90°); J) $\Delta R/R_0$ change of HDP

2

574 hydrogel of making expressions (frowning and astonishment) and K) speaking different words; L)

575 $\Delta R/R_0$ change of HDP hydrogel during bending the knee and M) the wrist before and after self-

576 healing.

577

578 *3.5. On-body epidermal and in vivo electrophysiology signals monitoring*

579 To further demonstrate the potentiality of HA-DA-PP hydrogels within epidermal and

580 *in vivo* electrophysiology signals monitoring, the biocompatibility was firstly assessed

581 via co-culture with 3T3 cells in **Figure S8 &9**. Both Live/Dead staining and MTT

582 analysis showed the good biocompatibility of HA-DA-PP hydrogels. Subsequently, the

583 epidermal signal detection performance of HDP hydrogel was evaluated by filling it

584 into a commercial button-like electrode, then adhered onto the chest of a volunteer

585 (**Figure 5A**). As expected, the ECG signals can be detected, showing clearly R, S, T, P,

586 Q peaks (**Figure 5B, S10**). **Figure 5C** illustrated the EMG signals of biceps muscle

587 during multiple static contraction. Similarly, HDP hydrogel showed a decent potential

588 for EEG signals detecting, as the EEG signals recorded by HDP hydrogel showed more

589 sensitive voltage amplitude and clearer details compared to the commercial hydrogel

590 electrode (**Figure 5D**).

591

592 The *in vivo* biocompatibility of HA-DA-PP hydrogel was further evaluated by dorsal

593 subcutaneous implantation in a SD rat model for 14 days. The histological assessments

594 based on hematoxylin and eosin staining (H&E) staining showed that a number of

595 inflammatory cells could be observed at the implantation interface of Ag group, while

596 HDP hydrogel did not cause obvious inflammatory reaction in subcutaneous tissues and

597 major organs **(Figure S11)**. Coming from the excellent biocompatibility, HA-DA-PP

598 hydrogel is promising for *in vivo* application scenarios. In situ sciatic, epicardial ECG

599 and ECoG signals recording via a rat model were then performed. For sciatic signal

600 recording, HDP hydrogel was wrapped on sciatic nerve, then the paws of rats were

601 poked with tweezers, sciatic signals after stimulation were clearly recorded (**Figure 5E**).

602 For epicardial ECG signal, HDP hydrogel was attached onto the epicardial surface

603 directly which can effectively avoid the high-amplitude noise from the heartbeat, then

604 the clear curve was observed (**Figure 5F**). It's worth noting that the epicardial ECG

605 curve does not occur any observable arrhythmia signs, also demonstrating the good

606 biocompatibility of HDP hydrogel within electrically active tissues. We further

607 investigated the application of HDP hydrogel for biological electrical signal in epileptic

608 seizure model. Firstly, we constructed a rat's epileptic seizure model with 4-

609 aminopyridine (4-AP) injection. In the state of epilepsy, action potentials triggered by

610 abnormally firing neurons could synergistically generate ECoG signals which was

611 clearly recorded by our HDP hydrogel electrode (Ding et al., 2022) (**Figure 5G, S12**).

612 The ECoG signals in different stages (rest, early, and late) of epileptic seizure were

613 showed in **Figure 5H**. At rest state, ECoG amplitude maintained at a low level. After

614 an epileptic seizure, the ECoG amplitude obviously increased as epilepsy active form

615 early to late stage. At same time, the corresponding time spectrum reflected the

616 enhanced power of the spectrum resulting from the discharge of abnormal neurons. As

617 control, a silver electrode was used to record the ECoG signals in the same way **(Figure

618 5I)**. The recorded signal amplitude and energy change trends were basically consistent

619 with those of HDP group. To further compare the quality by the HDP hydrogel and

620 silver electrode, the recorded signals were filtered into different frequency domains (α,

621 β, γ), in which signal waves may be induced due to epilepsy. Compared to silver

622 electrode, the more obvious augmentation of ECoG signals and reduction of foundation

623 noise appeared within HDP group, owing to more close conformal contact between soft

624 adhesive hydrogel and brain interface **(Figure 5J&K)**.
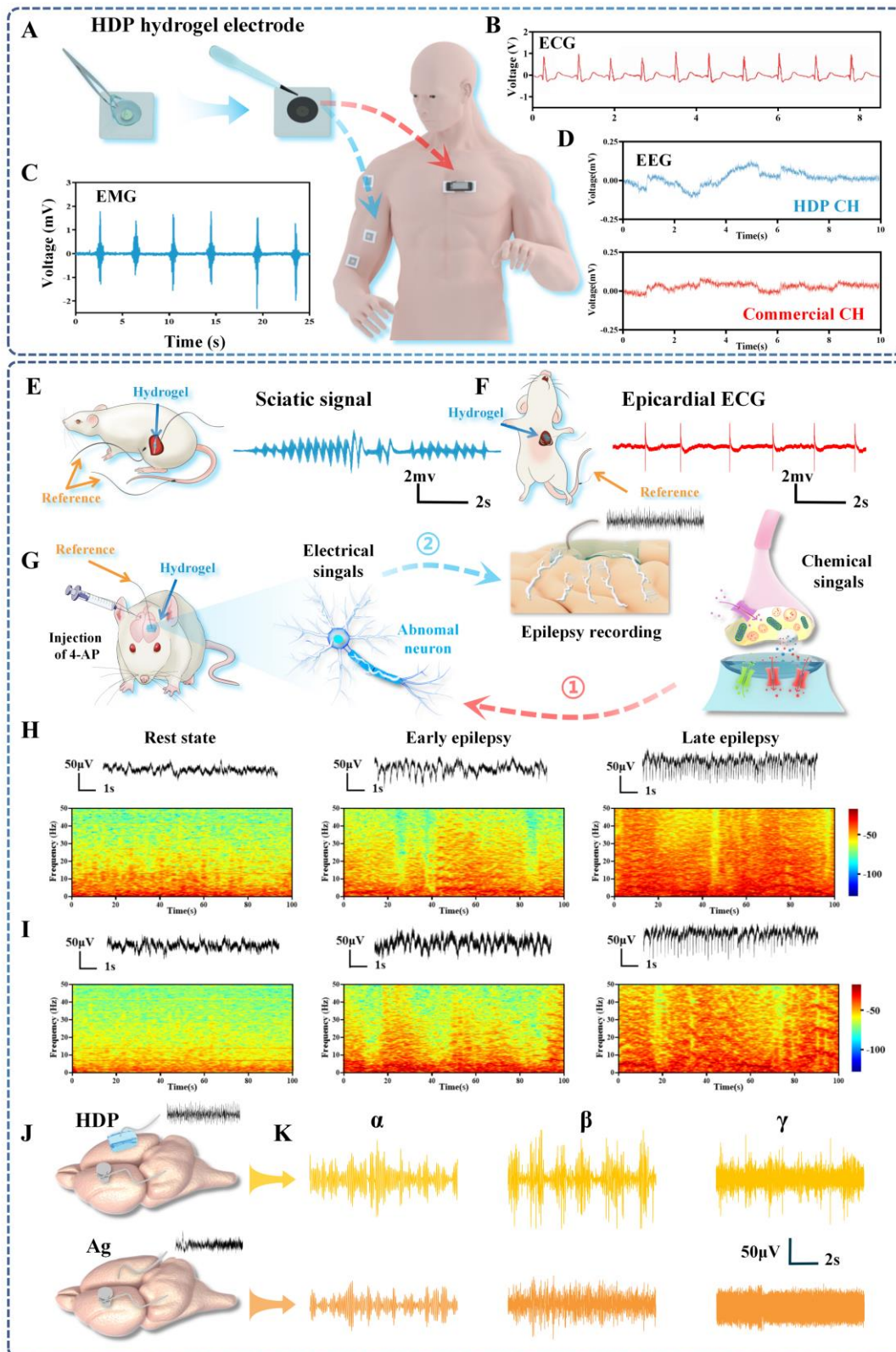
625

626 **Figure 5.** Application of HDP hydrogel in on-body epidermal and *in vivo* electrophysiology signals

627 monitoring. A) The preparation process of HDP-contained hydrogel electrode by filling it into a

2

628 commercial button-like electrode; B) ECG signal where obtained from the HDP-contained hydrogel

629 electrode adhering on the chest of a volunteer; C) EMG signals of biceps muscle during multiple

630 static contraction; D) EEG signals testing by HDP CH and the commercial CH; *in vivo* E) sciatic

631 and F) epicardial ECG recording by HDP hydrogel within a rat model; G) schematic diagram of the

632 ECoG signal recording within a 4-AP-induced epileptic rat model; ECoG signals (raw local field

633 potential, top; time-frequency spectrogram, bottom) recorded by H) HDP and I) silver wire in

634 different periods; J) schematic diagram of silver wire and HDP hydrogel as recording electrodes,

635 respectively; K) ECoG signals filtered into different frequency domains (α, β, γ) measured with

636 HDP hydrogel and silver wire during late epilepsy.

637

638 **4. Conclusion**

639 In summary, we developed a particle-free DA-introduced CH with favorable flexible

640 mechanical performances, high conductivity and good biocompatibility for human

641 motion monitoring, epidermal and *in vivo* electrophysiology signals monitoring. The

642 multiple interactions between PP-DA and HA-DA contributes not only the homogenous

643 distribution of conductive PP in HA-based hydrogel network, effectively avoids stress

644 concentration around conductive NPs, but also results in high stretchability (over

645 470%), tissue-adhesiveness and self-healing capability. Meanwhile, in addition to the

646 introducing of conductive phase, interaction between DA and PEDOT of

647 conformational transition and charge transfer effects greatly improves the conductivity

648 of HA-DA-PP hydrogel. Furthermore, profiting from the excellent conductivity and

649 biocompatibility, HA-DA-PP hydrogel realizes real-time monitoring of human

650 movements, as well as on-body epidermal and *in vivo* electrophysiology signals

651 monitoring, with augmented signals and reduced noise. Overall, this work provides a

652 universal paradigm of designing multifunctional materials for flexible epidermal

653 sensors, and reliable implantable electrophysiological monitoring.

654

655 **CRediT authorship contribution statement**

Ming-Ze Zeng: Investigation, Methodology, Data curation, Formal analysis, Writing - original draft. **Dan Wei**: Conceptualization, Investigation, Data curation, Writing - review & editing, Funding acquisition. **Jie Ding**: Conceptualization, Methodology. Yuan Tian: Software, Data curation. **Yuan Tian**: Visualization. **Xiao-Yang Wu**: Collection of some experimental data. **Zhi-Hong Chen:** Collection of some experimental data. **Cheng-Heng Wu**: Conceptualization. **Jing Sun**: Writing - review & editing. **Hua-Bing Yin**: Conceptualization, Results discussion. **Hong-Song Fan**: Conceptualization, Writing - review & editing, Funding acquisition, Project administration.

Declaration of competing interest

The authors declare no conflict of interest.

Data availability

Data will be made available on request.

Appendix A. Supplementary data

The following is the Supplementary data to this article:

References

684   Abatangelo, G., Vindigni, V., Avruscio, G., Pandis, L., & Brun, P. (2020). Hyaluronic acid:
685   redefining its role. *Cells,* 9(7), 1743.

686   Chen, S., Liu, A., Wu, C., Chen, Y., Liu, C., Zhang, Y., . . . (2021). Static–Dynamic Profited
687   Viscoelastic Hydrogels for Motor-Clutch-Regulated Neurogenesis. *ACS Applied Materials*
688   *& Interfaces,* 13(21), 24463-24476.

689   Chen, Z., Chen, Y., Hedenqvist, M. S., Chen, C., Cai, C., Li, H., . . . (2021). Multifunctional
690   conductive hydrogels and their applications as smart wearable devices. *Journal of*
691   *Materials Chemistry B*, 9(11), 2561-2583.

692   Ding, J., Chen, Z., Liu, X., Tian, Y., Jiang, J., Qiao, Z., . . . (2022). A mechanically adaptive hydrogel
693   neural interface based on silk fibroin for high-efficiency neural activity recording.
694   *Materials Horizons,* 9(8), 2215-2225.

695   Fan, X., Nie, W., Tsai, H., Wang, N., Huang, H., Cheng, Y., . . . (2019). PEDOT: PSS for flexible
696   and stretchable electronics: modifications, strategies, and applications. *Advanced Science,*
697   6(19), 1900813.

698   Gan, D., Huang, Z., Wang, X., Jiang, L., Wang, C., Zhu, M., . . . (2020). Graphene oxide-templated
699   conductive and redox-active nanosheets incorporated hydrogels for adhesive bioelectronics.
700   *Advanced Functional Materials,* 30(5), 1907678.

701   Ge, G., Yuan, W., Zhao, W., Lu, Y., Zhang, Y., Wang, W., . . . (2019). Highly stretchable and
702   autonomously healable epidermal sensor based on multi-functional hydrogel frameworks.
703   *Journal of Materials Chemistry A,* 7(11), 5949-5956.

704   Hassan, M., Abbas, G., Li, N., Afzal, A., Haider, Z., Ahmed, S., . . . (2022). Significance of flexible
705   substrates for wearable and implantable devices: Recent advances and perspectives.
706   *Advanced Materials Technologies,* 7(3), 2100773.

707   Highley, C. B., Prestwich, G. D., & Burdick, J. A. (2016). Recent advances in hyaluronic acid
708   hydrogels for biomedical applications. *Current opinion in biotechnology,* 40, 35-40.

709   Huang, H., Han, L., Fu, X., Wang, Y., Yang, Z., Pan, L., & Xu, M. (2020). Multiple stimuli
710   responsive and identifiable zwitterionic ionic conductive hydrogel for bionic electronic
711   skin. *Advanced Electronic Materials,* 6(7), 2000239.

712   Huang, J., Wang, K.-X., Chang, J.-J., Jiang, Y.-Y., Xiao, Q.-S., & Li, Y. (2017). Improving the
713   efficiency and stability of inverted perovskite solar cells with dopamine-copolymerized
714   PEDOT: PSS as a hole extraction layer. *Journal of Materials Chemistry A,* 5(26), 13817-
715   13822.

716   Jeong, W., Gwon, G., Ha, J.-H., Kim, D., Eom, K.-J., Park, J. H., . . . (2021). Enhancing the
717   conductivity of PEDOT: PSS films for biomedical applications via hydrothermal treatment.
718   *Biosensors and Bioelectronics,* 171, 112717.

719   Jia, Z., Gong, J., Zeng, Y., Ran, J., Liu, J., Wang, K., . . . (2021). Bioinspired conductive silk
720   microfiber integrated bioelectronic for diagnosis and wound healing in diabetes. *Advanced*
721   *Functional Materials,* 31(19), 2010461.

722   Lai, J. (2014). Relationship between structure and cytocompatibility of divinyl sulfone cross-linked
723   hyaluronic acid. *Carbohydrate polymers,* 101, 203-212.

724   Le, T.-H., Kim, Y., & Yoon, H. (2017). Electrical and electrochemical properties of conducting

polymers. *Polymers, 9*(4), 150.

Li, G., Li, C., Li, G., Yu, D., Song, Z., Wang, H., . . . (2022). Development of conductive hydrogels for fabricating flexible strain sensors. *Small, 18*(5), 2101518.

Li, H., Ma, Y., & Huang, Y. (2021). Material innovation and mechanics design for substrates and encapsulation of flexible electronics: a review. *Materials Horizons, 8*(2), 383-400.

Liang, Y., Zhao, X., Hu, T., Chen, B., Yin, Z., Ma, P. X., & Guo, B. (2019). Adhesive hemostatic conducting injectable composite hydrogels with sustained drug release and photothermal antibacterial activity to promote full-thickness skin regeneration during wound healing. *Small, 15*(12), 1900046.

Lin, T., Li, S., Hu, Y., Sheng, L., Chen, X., Que, X., . . . (2022). Ultrastretchable and adhesive agarose/Ti3C2Tx-crosslinked-polyacrylamide double-network hydrogel for strain sensor. *Carbohydrate polymers, 290*, 119506.

Liu, Q., Qiu, J., Yang, C., Zang, L., Zhang, G., & Sakai, E. (2021). High-performance PVA/PEDOT: PSS hydrogel electrode for all-gel-state flexible supercapacitors. *Advanced Materials Technologies, 6*(1), 2000919.

Liu, S., Zheng, R., Chen, S., Wu, Y., Liu, H., Wang, P., . . . (2018). A compliant, self-adhesive and self-healing wearable hydrogel as epidermal strain sensor. *Journal of Materials Chemistry C, 6*(15), 4183-4190.

Liu, X., Deng, J., Ma, L., Cheng, C., Nie, C., He, C., & Zhao, C. (2014). Catechol chemistry inspired approach to construct self-cross-linked polymer nanolayers as versatile biointerfaces. *Langmuir, 30*(49), 14905-14915.

Namsheer, K., & Rout, C. S. (2021). Conducting polymers: A comprehensive review on recent advances in synthesis, properties and applications. *RSC advances, 11*(10), 5659-5697.

Pang, Y., Zhang, K., Yang, Z., Jiang, S., Ju, Z., Li, Y., . . . (2018). Epidermis microstructure inspired graphene pressure sensor with random distributed spinosum for high sensitivity and large linearity. *ACS nano, 12*(3), 2346-2354.

Park, J., Lee, Y., Barbee, M. H., Cho, S., Cho, S., Shanker, R., . . . (2019). A hierarchical nanoparticle-in-micropore architecture for enhanced mechanosensitivity and stretchability in mechanochromic electronic skins. *Advanced Materials, 31*(25), 1808148.

Rudd, S., & Evans, D. (2022). Recent advances in the aqueous applications of PEDOT. *Nanoscale Advances*, 4, 733-741.

Shi, Z., Gao, X., Ullah, M. W., Li, S., Wang, Q., & Yang, G. (2016). Electroconductive natural polymer-based hydrogels. *Biomaterials, 111*, 40-54.

Song, X., Wang, X., Zhang, J., Shen, S., Yin, W., Ye, G., . . . (2021). A tunable self-healing ionic hydrogel with microscopic homogeneous conductivity as a cardiac patch for myocardial infarction repair. *Biomaterials, 273*, 120811.

Sun, X., Agate, S., Salem, K. S., Lucia, L., & Pal, L. (2020). Hydrogel-based sensor networks: Compositions, properties, and applications—A review. *ACS Applied Bio Materials, 4*(1), 140-162.

Tang, W., Fu, C., Xia, L., Lyu, P., Li, L., Fu, Z., . . . (2022). A flexible and sensitive strain sensor with three-dimensional reticular structure using biomass Juncus effusus for monitoring human motions. *Chemical Engineering Journal, 438*, 135600.

767   Won, D., Kim, J., Choi, J., Kim, H., Han, S., Ha, I., . . . (2022). Digital selective transformation and
768   patterning of highly conductive hydrogel bioelectronics by laser-induced phase separation.
769   *Science Advances,* 8(23), 3209.

770   Xu, C., Chang, Y., Wu, P., Liu, K., Dong, X., Nie, A., . . . (2021). Two-Dimensional-Germanium
771   Phosphide-Reinforced Conductive and Biodegradable Hydrogel Scaffolds Enhance Spinal
772   Cord Injury Repair. *Advanced Functional Materials,* 31(41), 2104440.

773   Yang, J. C., Mun, J., Kwon, S. Y., Park, S., Bao, Z., & Park, S. (2019). Electronic skin: recent
774   progress and future prospects for skin-attachable devices for health monitoring, robotics,
775   and prosthetics. *Advanced Materials,* 31(48), 1904765.

776   Yazdi, M. K., Zarrintaj, P., Khodadadi, A., Arefi, A., Seidi, F., Shokrani, H., . . . (2021).
777   Polysaccharide-based electroconductive hydrogels: Structure, properties and applications
778   in biomedical engineering. *Carbohydrate Polymers*, 278, 118998.

779   Zeng, M., Wang, X., Ma, R., Zhu, W., Li, Y., Chen, Z., . . . (2020). Dopamine semiquinone radical
780   doped PEDOT: PSS: Enhanced conductivity, work function and performance in organic
781   solar cells. *Advanced Energy Materials,* 10(25), 2000743.

782